Dynamics of Dielectrophoretic Liquid Microactuation

T. B. Jones
Department of Electrical & Computer Engineering, University of Rochester, Rochester, NY 14627 (USA)
Email: jones@ece.rochester.edu

Abstract

Dielectrophoretic (DEP) liquid microactuation provides a controllable means for rapid movement and dispensing of small liquid volumes on a substrate. Applications in μTAS (micro total analysis systems) are envisioned. The microfluid mechanics of DEP actuation are complex and not entirely well understood, due to several factors including the strong influence of capillarity and surface wetting phenomena. In this paper, models are presented for the transient motion initiated when the voltage is turned on and for the stability of the electric-field-coupled hydrostatic equilibrium when the motion ceases. Field gradient stabilization and contact line pinning are two possible mechanisms for the observed stable behavior of the liquid configuration, though at present it is unclear which mechanism is more effective. The linearized hydrodynamic model for a rivulet is used to predict the dominant unstable wavelength and thence the size of the droplets formed when the electric field is removed. Droplet size reproducibility is vitally important in the practical application of DEP microactuation.

Keywords: dielectrophoresis, microfluidics, laboratory on a chip, rivulets, Maxwell stress tensor

INTRODUCTION

The last decade has seen significant strides in the development of μTAS (micro total analysis systems) technology [1]. This technology seeks to replace conventional test tubes, well plates, capillaries, micropipettes, and even cumbersome diagnostic equipment such as liquid chromatographs with a revolutionary concept, the *laboratory on a chip*. This new class of fully automated micro-reactors is based on microfabrication technology pioneering by the integrated circuit industry and recently exploited by MEMS (microelectromechanical systems). The laboratory on a chip features liquid handling structures placed side by side on a substrate with all necessary sensors, control instrumentation, and sophisticated chemical or bio-chemical diagnostic systems.

Chemists, biologists, and biomedical researchers envision many applications for this technology. In combinatorial chemistry, the ability to initiate and monitor large numbers of reactions under closely controlled conditions automatically using very small initial inventories of chemicals is understandably attractive. In the case of wet chemistry, mixing and reaction times are significantly shorter when liquid inventories are small. From the cost standpoint, the benefit of using reduced amounts of chemicals is evident, while from the safety standpoint, automation can minimize worker handling and exposure to dangerous substances. Furthermore, the small inventory requirement (nanoliters or less) might be beneficial in biomedical research when only very tiny quantities of rare cells can be isolated.

Most μTAS concepts rely on some means for controlled movement of small liquid volumes around on a substrate. Distributed forces, including capillarity [2] and surface wetting [3], electro-osmosis [4], electroconvection [5], and electrowetting [6] are under consideration, and recently, dielectrophoresis (DEP) has been proposed [7]. The demonstrated advantage of DEP actuation is the speed at which liquid volumes can be transported and dispensed, and so now there is a need to develop improved predictive models for microdielectrophoretic liquid actuation. In this paper, we report progress made in understanding these interesting microfluid dynamics.

MICROFLUIDICS

The laboratory on a chip requires a microfluidic "plumbing system," that is, some controllable means to move liquid around the substrate. There are two basically distinct types of such systems. To date, most effort has been devoted to "closed channel" microfluidic schemes. These structures are fabricated by machining deep channels into substrates and then covering or sealing them to form ducts or pipes open only at the ends, thorough which the liquid is pumped. To achieve adequate flow through such tiny structures, rather high pressure heads are required (up to 10^5 Pa). Production scale microfabrication of leak-free structures of such complexity is not without challenge. Other unsolved problems with closed channel microfluidics include (i) designing a reliable interface between these microstructures and the user and (ii) priming the pumps used to move liquid through the channels [8].

The other distinct type of microfluidic systems is "open channel" systems, where the liquid sits on the substrate. An obvious advantage of open structures is the accessibility of the liquid; injection and withdrawal of liquid seems simple. Furthermore, neither priming nor leakage problems exist, and their simple, virtually planar geometries should make fabrication easy. On the other hand, undesirable evaporation may require hermetic sealing.

Fluid control has been demonstrated using thermo-capillarity [9] and voltage-actuated surface wetting [10]. Such schemes show promise in dispensing extremely small volumes with good accuracy; however, capillary-driven microfluidic flows are inherently very slow. On the other hand, DEP liquid actuation is fast. Liquid fronts can be driven at speeds up to ~25 cm/s, and multiple liquid droplets of volumes down to ~1 nanoliter (and probably much less)

can be dispensed from microliter volumes in less than 0.1 s. In this paper we describe an effort to create practical predictive models for the transient dynamics of DEP microactuation. A simple model for the transient dynamics of an advancing finger is presented and its predictions then compared to experiment. Also, a hydrodynamic model for a DEP-stabilized rivulet is described and compared to limited droplet-formation experiments.

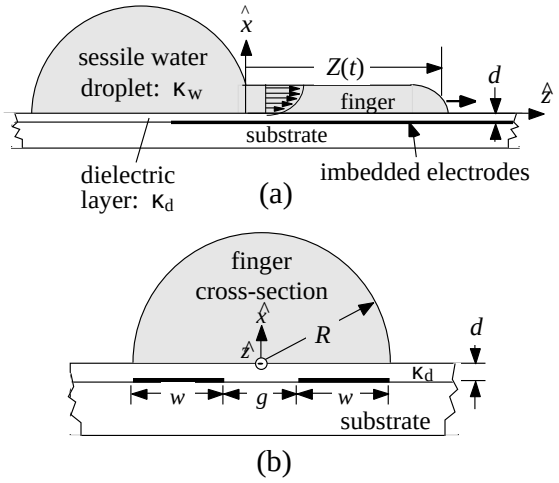

Fig. 1 Simple model for water finger extending from a large droplet. (a) Side view with definitions for $Z(t)$ and other quantities. (b) Semi-circular cross-section of finger of radius R and substrate showing location of electrodes and dielectric layer of thickness d and dielectric constant κ_d.

DYNAMIC MODEL FOR FINGER MOVEMENT

Fig. 1a depicts the physical model for a liquid finger projecting from a microliter-sized sessile droplet when voltage V is applied. The finger moves along parallel, coplanar electrodes patterned from evaporated metal on an insulating substrate. The electrodes, of uniform width w and spacing g, are coated by polyimide having dielectric constant κ_d and thickness d. If the z-directed DEP force f^e is large enough to overcome surface tension, the finger emerges from the droplet and moves along the electrode structure. There is a minimum frequency required to achieve the desired compact liquid profile [7]. It is observed that, as the finger lengthens, it retains a virtually uniform, essentially semicircular cross-sectional profile. Therefore, our dynamic model assumes the profile to be a semicircle of radius R, centered upon the gap and overlapping the electrodes as shown in Fig 1b.

Resisting the DEP force are the surface tension and viscous forces, f_γ and f_μ, respectively. To write the equation of motion, all forces are summed and equated to the rate of change of momentum of the finger, which has time-dependent length $Z(t)$. Because the cross-section of the finger is assumed constant, the water drawn into it from the sessile droplet must accelerate very rapidly to a fully developed velocity profile having average velocity equal to dZ/dt.

$$\frac{\pi \rho R^2}{2}\frac{d}{dt}\left(Z\frac{dZ}{dt}\right) = f^e + f_\gamma + f_\mu \qquad (1)$$

The DEP force

The assumption that the finger profile is fixed permits use of a lumped parameter electromechanical model to calculate f^e. This approach precludes any need for detailed knowledge of the electric field near the leading edge of the finger. If the profile assumes the configuration shown in Fig. 1b, and if $d \ll w$ and g, then the total system capacitance is

$$C(Z) = \frac{Z}{1/\kappa_w c_{air} + 2/c_d} + \frac{L - Z}{1/c_{air} + 2/c_d} + C_{drop} \qquad (2)$$

where L is the total length of the electrodes not covered by the droplet, κ_w is the dielectric constant of water, and C_{drop} is the essentially constant capacitance of the portion of the electrodes covered by the sessile droplet. The capacitances per unit length used in Eq. (2) are [7]

$$c_d \approx \kappa_d \varepsilon_o \, w/d \;\; \& \qquad (3)$$

$$c_{air} \approx \varepsilon_o K(1 - k^2)/2K(k^2)$$

$K(k^2)$ and $K(1- k^2)$ are complete elliptical integrals of the first kind, and $k^2 = (g/2R)^2$. These expressions are accurate if $d \ll g, w$. Using the principle of virtual work [11], the DEP force pulling the finger in the z direction is

$$f^e = \frac{V^2}{2}\frac{dC}{dZ} \qquad (4)$$

where V is the rms magnitude of voltage. Substituting Eq. (2) into Eq. (4) yields

$$f^e = \frac{(\kappa_w - 1)c_d^2 \, c_{air} \, V^2}{2(c_d + 2\kappa_w c_{air})(c_d + 2c_{air})} \qquad (5)$$

Capillary force

Surface tension impedes the finger's extension. If the cross-section is constant along the length of the finger, then this force is also constant and equal to the product of the semi-circular perimeter of the finger, πR, and the surface tension, γ.

$$f_\gamma = -\pi R \gamma \qquad (6)$$

Viscous force

The viscous force, which resists motion, may be expressed quite generally as the product of the total wetted base area of the finger, $2RZ(t)$, and the shear stress τ_μ exerted by the liquid on the substrate.

$$f_\mu \approx -2RZ\tau_\mu \qquad (7)$$

Estimates for the Reynolds number based on observed finger velocities indicate laminar flow. Then, again drawing on the assumption that the cross-section is uniform, one may argue that τ_μ is proportional to the velocity of the tip of the finger.

$$\tau_\mu \approx \frac{D\mu}{R}\frac{dZ}{dt} \qquad (8)$$

D is a dimensionless coefficient to be determined from the velocity profile.

Equation of motion

Substituting Eqs. (7) and (8) into Eq. (1) and doing some rearranging, one obtains

$$\frac{d^2 Z^2}{dt^2} + \frac{1}{T_\mu}\frac{dZ^2}{dt} = \frac{f^e + f_\gamma}{\rho\,\pi R^2/4} \qquad (9)$$

$T_\mu = \rho\pi R^2/4\mu D$ is a characteristic time that delineates the boundary between viscous and inertia-dominated behavior. If the voltage is applied at $t = 0$ and if we establish $Z(t = 0) = 0$ as an initial condition, the solution takes the following form.

$$Z(t) = \sqrt{\frac{T_\mu (f^e + f_\gamma)}{\rho\,\pi R^2/4}\left[t + T_\mu\,(e^{-t/T_\mu} - 1)\right]} \qquad (10)$$

According to this solution, $dZ/dt \neq 0$ at $t = 0_+$, which is not a violation of realizability because the finger is massless at $t = 0_+$.

For times short or long with respect to T_μ, the solution of Eq. (10) may be simplified:

$$Z(t) \approx \begin{cases} \sqrt{\dfrac{f^e + f_\gamma}{\pi\rho R^2/2}}\,t, & t << T_\mu \\ \sqrt{\dfrac{T_\mu (f^e + f_\gamma)}{\pi\rho R^2/4}}\,t, & t >> T_\mu \end{cases} \qquad (11)$$

For $t << T_\mu$, the dynamics are controlled by inertia, while for $t >> T_\mu$, viscosity dominates. In the case of DEP microfluidics, viscosity dominates for all practical time scales.

Minimum voltage for finger formation

The finger will not move unless the DEP force exceeds the surface tension force. Therefore, the condition $f^e = -f_\gamma$ allows us to determine the minimum voltage required for DEP liquid actuation.

$$V_{min} = \sqrt{\frac{2\pi\gamma R(c_d + 2\kappa_w c_{air})(c_d + 2c_{air})}{(\kappa_w - 1)\,c_d^2\,c_{air}}} \qquad (12)$$

Fig. 2 plots V_{min} versus finger radius R under the parameter specification $g = w = 2R/3$ for selected values of d. Table 1 contains relevant material properties for water and polyimide used in the calculations.

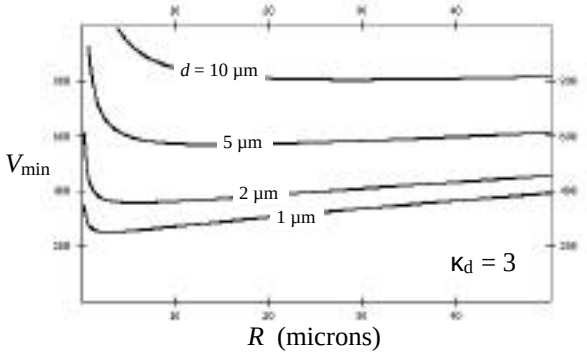

Fig. 2 Minimum voltage for DEP actuation, V_{min} from Eq. (12), plotted versus finger radius R, with $g = w = 2R/3$ for d = 1, 2, 5, and 10 µm.

quantity	value
dielectric constant of polyimide, κ_d	~3
dielectric constant of water, κ_w	80
surface tension of water, γ	0.073 Nt/m
contact angle of water on polyimide, θ	~75°
mass density of water, ρ	1000 kg/m^3
viscosity of water, μ	0.001 Nt-s/m^2

Table 1. Material properties of water & polyimide (23° C).

Joule heating makes it almost impossible to determine V_{min} experimentally; however, limited comparisons of measured to calculated V_{min} values can be made. For electrode structures with dimensions g = 20 µm, w = 20 µm, and d = 10 µm, the experimentally determined voltage for actuation is ~500 V. On the other hand, the d = 10 µm curve in Fig. 2 predicts $V_{min} \geq 800$ V. There are several likely sources of error in the model that could explain this discrepancy. One problem is the approximate nature of the capacitance expressions, which may suffer inaccuracy, given the fact that the $d << w,g$ condition is not met. Furthermore, all values for dielectric thickness d are estimates obtained from an empirical process equation rather than measurement.

Dynamic model with viscosity

To estimate the viscosity coefficient D, we assume the no-slip condition at the substrate ($x = 0$) and approximate the x-directed laminar flow of liquid in the semi-circular cross-section of the finger by a Poiseuille-like velocity profile [12].

$$v(x,t) = v_{max}\left[2\left(\frac{x}{R}\right) - \left(\frac{x}{R}\right)^2\right] \qquad (13)$$

The volume flow averaged liquid velocity v_{avg} is set equal to the finger velocity.

$$v_{avg} = 0.599\,v_{max} \equiv \frac{dZ}{dt} \qquad (14)$$

Then, using the definition for viscous shear stress

$$\tau_\mu = \mu\frac{\partial v}{\partial x} \qquad (15)$$

the viscosity coefficient is found to be D = 3.33. Figs. 3a and b plot finger length Z and velocity dZ/dt, respectively, versus time t for parameter sets comparable to experiment. The calculated time constant T_μ never exceeds ~10^{-4} s, signifying that the finger dynamics are viscosity-limited.

Comparison to experiment

Fig. 4 contains a plot of experimental data for finger length Z versus time t, obtained from a videotape recorded at 1125 frames per second, for a flow structure having the following parameters: $w = g$ = 20 µm, $R \approx$ 30 µm, and $V \approx$ 700 V-rms. To calculate the superimposed theoretical curve from Eq. (10), we used these same electrode dimensions, but treated κ_d, the dielectric constant of the insulating layer, as an

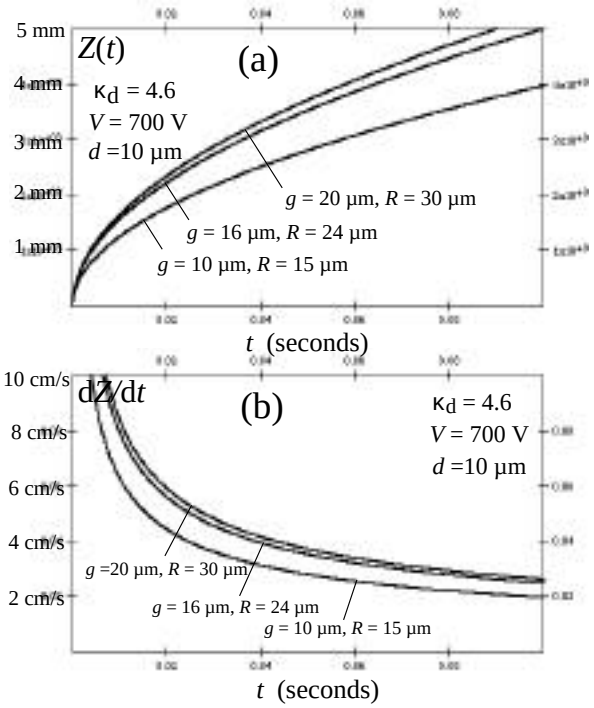

Fig. 3 Time dependence of finger length $Z(t)$ and tip velocity dZ/dt for R = 15 μm, 24 μm, and 30 μm, $g = w = 2R/3$, d = 10 μm, and V = 900 v. Material parameters from Table 1 used.

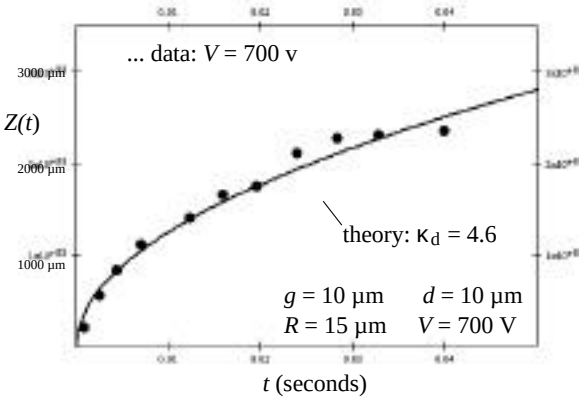

Fig. 4 Plot of finger length $Z(t)$ data and theory versus time t for $g = w = 2R/3$, R = 30 μm, and d = 10 μm. Dielectric constant κ_d is used here as an adjustable parameter to fit the theory to the experimental data.

adjustable parameter. The value $\kappa_d = 4.6$ seems to give the best fit, though $\kappa_d = 3$ is a more accurate value for spin-coated polyimide. A justification for treating κ_d as the adjustable parameter is that the predicted electric field in the dielectric layer (E_b ~ 100 V/μm) exceeds the breakdown strength of polyimide. Rf breakdown in the layer would increase the actual voltage drop in the water above its predicted value so that Eq. (5) would under-estimate f^e. Adjusting the value of κ_d upward, as done here, has the same effect of increasing the portion of the voltage drop occurring in the finger.

FINGER STABILITY

Practical utilization of DEP microactuation inevitably involves transient motion of a finger moving along a flow structure. But when the finger reaches the end of a structure, motion stops and stable, hydrostatic equilibrium, governed by a balance of electrical and surface tension forces, becomes established. When the voltage is removed, hydrodynamic instability, closely related to the well-known capillary jet instability [13], breaks up the finger into droplets within ~10^{-3} s. Understanding this instability, and how the electric field actually suppresses it, is crucial to DEP microfluidics schemes if accurate, reproducible dispensing of droplets is to be achieved.

Observations

Fig. 5 shows a sequence of high-speed videomicrographs (1125 fps) of an electrode structure with four adjacent pairs of evenly spaced semi-circles intended to promote droplet formation. In these experiments, w = 20 μm, g = 20 μm, and $R \approx$ 30 μm. The diameters of the circles are ~150 μm and their center-to-center spacing is 550 μm. In Fig. 5a, the finger has reached the end of the structure, flow has stopped and the voltage (~600 V @ 100 kHz) has been turned on for ~1 s. The finger is stable. In Fig. 5b, the voltage has just been turned off and the capillary instability is proceeding, while in 5c the instability has run its course, forming a ~1.4 (±25%) nanoliter droplet at each circle. Note the very small satellite droplets (~50 picoliters) midway between the circles.

It is apparent that the electric field, which initially draws the liquid finger forward from the sessile droplet, creates a stable hydrostatic equilibrium, once the structure has filled and flow stopped. Upon removal of the field, instability ensues immediately,

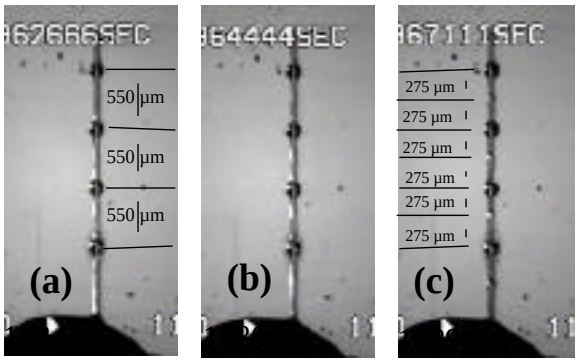

Fig. 5 Micrographs from videotape sequence taken at 1125 fps, showing hydrodynamic instability and consequent nanodroplet formation after removal of electric field (d = 10 μm, w = 20 μm. g = 20 μm, $R \approx$ 30 μm); de-ionized water used. a) Voltage on; finger is not in motion and is hydrodynamically stable; b) Voltage off; instability is proceeding; c) Voltage off; regularly-spaced droplets (~1.4 nl) and satellites (<0.05 nl) have formed in <0.004 s.

leading to formation of the nanoliter droplets at the circular electrodes, and the much smaller droplets midway between them.

Theory

Rivulets, narrow liquid channels flowing on a solid surface, are strongly influenced by surface wetting. Davis proposed two distinct boundary constraints to account for this wetting: (i) fixed wetting angle (θ) and (ii) fixed contact lines [14]. For the first case, he found that there always exists a range of unstable wavelengths. On the other hand, if the contact lines are pinned in place, he showed that stability depends on the value of the wetting angle, viz.: for $\theta < 90^o$, the equilibrium is stable for all wavelengths; for $\theta > 90^o$, wavelengths greater than some value are always unstable.

Davis's model can be exploited to provide useful insights about DEP microactuation. For example, when the electric field is present, the finger is stable and strong pinning of the contact lines immediately above either both inner or both outer edges of the strip electrodes is observed [15]. The natural contact angle for water resting on polyimide is $\theta \approx 75^o$. Therefore, if the only effect of the non-uniform electric field were to pin the liquid contact lines, then, according to Davis's model, the finger would be stable. However, there is another possible stabilizing mechanism, namely, the non-uniform field which can control a liquid interface if the field gradient is properly oriented [16]. The problem is to determine which mechanism of stabilization is effective.

Schiaffino and Sonin [17] provide a simplified, inviscid theory for the linear dynamics of rivulets based upon the work of Davis, which can be modified readily to determine the effectiveness of gradient stabilization. Further, their unmodified theory can be used to delineate the range of unstable wavelengths after the electric field has been removed. The important matters of droplet volume reproducibility and the lower limit imposed upon droplet size depend critically on this range of unstable wavelengths.

Electric field stabilization of water finger

To model the surface wave dynamics of the water finger, we modify Schiaffino and Sonin's theory by addition of an electric surface traction to the pressure term. Refer to the Appendix.

$$\rho\left(\frac{\partial v}{\partial t} + v\frac{\partial v}{\partial z}\right) = -\frac{\partial}{\partial z}\left[\gamma\left(\frac{1}{R} + \frac{1}{R'}\right) - \frac{(\varepsilon_w - \varepsilon_o)}{2} E_\phi^2\right] \qquad (16)$$

R is already defined in Fig. 1b, R' is the radius of curvature of the surface along the z-axis, and v is the z-directed velocity perturbation. We approximate the primarily tangential electric field at the interface by

$$E_\phi \approx V_w / \pi R \qquad (17)$$

V_w is the net voltage drop occurring within the water. Note that Eq. (17) is only accurate if the effective contact angle is close to 90º. Linearizing Eq. (16) to describe small longitudinal perturbations, we obtain

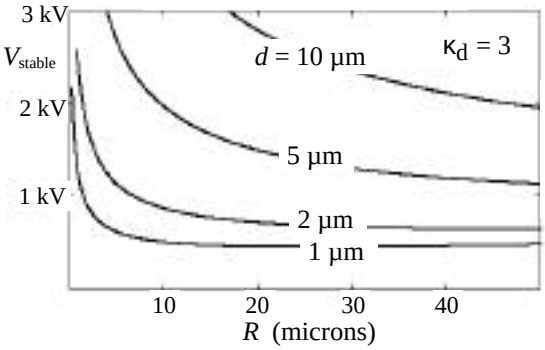

Fig. 6 Minimum voltage for stabilizing the water finger with respect to capillary instability, V_{stable} from Eq. (19), plotted versus finger radius R, with $g = w = 2R/3$ and d = 1, 2, 5, and 10 µm.

$$\rho\frac{\partial v}{\partial t} = \left[\frac{\gamma}{R^2} - \frac{(\varepsilon_w - \varepsilon_o)V_w^2}{2\pi^2 R^3}\frac{dR}{dh}\right]\frac{\partial h}{\partial z} + \beta(\theta)\gamma\frac{\partial^3 h}{\partial z^3} \qquad (18)$$

Here, $h(z,t)$ is a perturbation to the cross-sectional radius of the finger, while $\beta(\theta)$ is a factor used by Schiaffino and Sonin to correct for the influence of the liquid contact angle on the way R' is approximated. To ascertain the influence of the electric field on finger stability, it is necessary only to examine the term in brackets on the right side of Eq. (18). Note that neither β nor dR/dh influences this term. If the voltage is high enough so that the bracketed term is positive, capillary instability is suppressed for all wavelengths.

Setting the bracketed term in Eq. (18) to zero and using the capacitive voltage divider relationship, we obtain an expression for the value of the applied voltage required for stability.

$$V_{stable} = \frac{c_d + 2\kappa_w c_{air}}{c_d}\sqrt{\frac{2\pi^2 R\gamma}{(\varepsilon_w - \varepsilon_o)}} \qquad (19)$$

V_{stable} is plotted versus R in Fig. 6 for the condition $w = g = 2R/3$ and $\kappa_d = 3$. Even using the "adjusted" value $\kappa_d = 4.6$ from Fig. 4, $V_{stable} \sim 1600$ V, much higher than the experimentally observed value of ~600 (±100) V. The uncertainty of the capacitance expressions can not be discounted here. But another plausible explanation for the observed stability is pinning of the contact lines by the intense electric field above the edges of the electrodes. Further work is needed to test this contact line pinning hypothesis.

Finger instability after removal of E field

After the electric field is removed, capillary instability rapidly breaks up the finger into droplets. According to the conventional model for capillary jets, droplet size is determined by the fastest growing wavelength λ^*, so that, if the profile has the semi-circular shape shown in Fig. 1b, then we have $v_{drop} \approx$

$\pi R^2 \lambda_{expt}/2$. With no electric field present, one might argue that Davis's constant contact angle constraint is enforced while the instability progresses. Then, the predictive relations for the minimum and most unstable (fastest growing) wavelengths, λ_{min} and λ^* are [17]

$$\lambda_{min} \approx 3\pi R/\theta, \lambda^* = 2\pi R\sqrt{2\beta(\theta)(1-\cos\theta)} \quad (20)$$

The expression for λ_{min} is a straight-line approximation, accurate to ±5% for $\theta < 3\pi/4$, fitted to the plotted curve in Schiaffino and Sonin's paper. Using $\theta = 75^o$ and R = 30 μm in Eq. (20), we obtain λ_{min} = 108 μm and λ^* = 190 μm.

The question is whether or not the complex droplet formation phenomenon revealed in Fig. 5c can be explained by such a simple model. If we assume that the spatially periodic boundary conditions imposed by the droplet-forming circles limit the allowable wavelengths to a discrete set of values

$$\lambda_{unstable,n} = \Delta L/n \quad (21)$$

where n is an integer and ΔL = 550 μm, then the observed spacing between alternating large and small droplets, 275 μm, is consistent with n = 2. This value does not turn out to be the allowable wavelength closest to λ^* = 190 μm. The prediction would actually be λ = 183 μm, corresponding to n = 3. This discrepancy may be attributable to the fact that R has been measured with the voltage turned on, whereas the Eqs. (20) are in fact applicable with the voltage off.

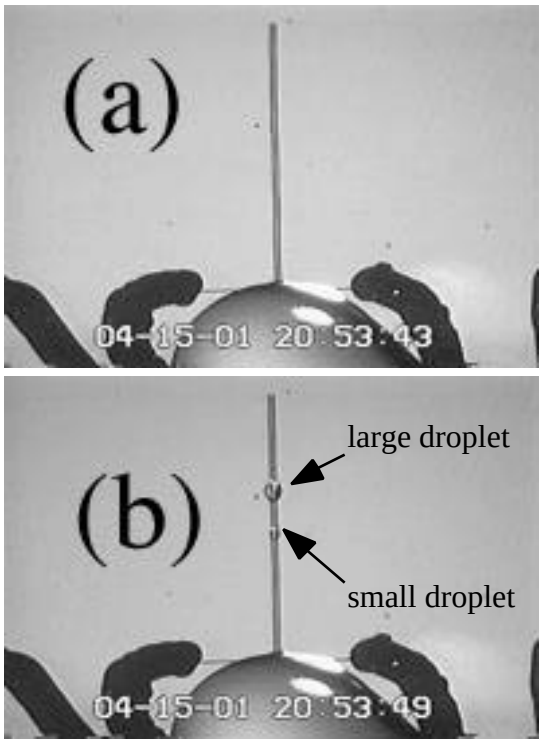

Fig. 7 Micrographs from videotape of droplet formation with de-ionized water using a straight electrode structure of length 2000 μm: d = 10 μm, w = 20 μm. g = 20 μm. a) Before removal of voltage; b) after removal of voltage. Two droplets of estimated volumes ~820 and ~93 picoliters are visible. Most of the water has been drawn back into parent drop visible at bottom of image.

Results obtained from a separate experiment cast further doubt on the simple model of the rivulet's instability after the electric field is removed. Fig. 7a,b show images from a video of an experiment conducted with a straight flow structure (w = g = 20 μm), containing no droplet-forming circles. Fig. 7b reveals that, when the electric field is removed, irregular droplets form with no discernible pattern. The two droplets visible have volumes estimated at ~820 and ~93 picoliters. For a structure with these dimensions, Eq. (20) predicts λ^* = 190 μm. Therefore, if the rivulet were to break up according to the conventional hypothesis for a capillary jet, then we might expect 2000/190 ≈ 10 droplets to form, each about 200 picoliters in volume. Because only the two droplets are observed when the electric field is removed, we must assume that considerable liquid has been drawn back into the large droplet at the bottom of the image. Such motion, ensuing immediately after the electric field is turned off, would destroy the hydrostatic equilibrium upon which our hydrodynamic theory is based.

CONCLUSION

DEP microactuation uses planar electrodes, fabricated using conventional photolithography, to exert a dielectrophoretic force on polarizable liquids (such as water). We can exploit this force to manipulate small liquid volumes very rapidly and to divide them into smaller volumes. The leading edge of the narrow water finger protruding from a large sessile droplet on a substrate moves as fast as ~25 cm/s. Some combination of the DEP force and possible contact line pinning restricts the finger to a stable, compact, semicircular profile as it lengthens. Using energy methods to compute the DEP driving force, we have developed a simple model to predict this rapid motion. The model gives $Z(t)$ $t^{0.5}$, which predicts with fair success the slow deceleration of the transient motion as the finger lengthens. A capacitive voltage divider expression is used to determine the electric field acting on the water finger, and it is likely that errors in the capacitance expressions lead to underestimation of the electric fields within the water.

The behavior of the water finger after it reaches the end of an electrode flow structure and stops is, in importance, at least equal to the transient response. When the electric field is present, the finger is observed to be stable. We have modified Schiaffino and Sonin's linear hydrodynamic model for a rivulet [17] to account for the effect of the non-uniform electric field on the stability. The result is inconclusive as to whether or not gradient stabilization suppresses the capillary instability by itself. A different mechanism, where the locally

intense field above the edges of the electrodes pins the contact lines of the rivulet, may be just as effective.

Vallet et al. reported localized electrical breakdown along the contact line of a spreading liquid film [18]. This breakdown influences the film dynamics by irreversible alteration of the wetting property of the substrate, viz., the surface becomes more hydrophilic. The effect is observed at a voltage similar to DEP actuation, ~1 kV, but at a much lower frequency, ~1 kHz instead of ~100 kHz. Further effort to investigate questions about contact line pinning and surface alteration is essential, not because of uncertainty about finger stability, but because, if contact line pinning does occur, we need to understand it.

When the rf electric field is removed, the finger breaks up rapidly into droplets on a time scale of order 10^{-3} s. Schiaffino and Sonin's theory in its unmodified form should predict the wavelengths of instability; however, our experiments provide ambiguous evidence. For a structure with regularly spaced, droplet forming circles, there is evidence supporting the "most unstable wavelength" hypothesis familiar from capillary jet theory. On the other hand, droplet formation on straight electrode structures, that is, with no structural periodicity imposed by droplet forming circles, is very irregular and unpredictable. A possible explanation for this behavior is that, as soon as the voltage is removed, the finger starts to retract. This motion disrupts the hydrostatic equilibrium just as the capillary instability gets underway. If DEP microactuation is ever to provide precise delivery and repeatable droplet dispensing for application in the laboratory on a chip, further research is required to resolve these questions.

ACKNOWLEDGMENT

The author acknowledges support from the Japan Society for the Promotion of Science, the US National Science Foundation (Center for Global Partnership), the Center for Future Health (University of Rochester), and the National Institutes of Health. He is grateful to Prof. M. Washizu of Kyoto University for the hospitality extended to him during a sabbatical in 2000. Mr. M. Gunji of Kyoto University obtained the videos for the images in Figs. 5 and 7.

REFERENCES

1. N. Giordano and J-T. Cheng, *J. Phys.: Condensed Matter*, **13**, R271-R295 (2000).
2. D. J. Harrison, K. Fluri, Z. Fan, and K. Seiler, in *Micro Total Analysis Systems*, A. Van Den Berg and P. Bergveld, eds. (Kluwer: Dortrecht, NL), 105-115 (1995).
3. H. Gau, S. Herminghaus, P. Lenz, and R. Lipowsky, *Science* **283**, 46-49 (1999).
4. D.C. Duffy, O. J. Schueller, O. J. A. Brittain, and G. M. Whitesides, J. Micromech. Microeng., **9**, 211-217 (1999)
5. S. E. McBride, R. M. Moroney, and W. Chiang, in Micro Total Analysis Systems '98, D. J. Harrison and A. Van Den Berg, eds. (Kluwer: Dortrecht, NL), 45-48 (1998).
6. J. A. M. Sondag-Huethorst and L. G. L. Fokkink, J. Electroanal. Chem. **367** (1994) 49-57; M. G. Pollack, R. B. Fair, A. D. Shenderov, *Applied Physics. Lett.* **77**, 1725-1726 (2000).
7. T. B. Jones, M. Gunji, M. Washizu, and M. J. Feldman, *J. Applied Physics* **89**, 1441-1448 (2001).
8. D. J. Harrison, Preface, in Micro Total Analysis Systems '98, D. J. Harrison and A. Van Den Berg, eds. (Kluwer: Dortrecht, NL), iii (1998).
9. D. E. Kataoka and S. M. Troian, *Nature* **402**, 794-797 (1999).
10. B. S. Gallardo, V. K. Gupta, F. D. Eagerton, L. I. Jong, V. S. Craig, R. R. Shah, and N. L. Abbott, *Science* **283**, 57-60 (1999).
11. H. H. Woodson and J. R. Melcher, Electromechanical Dynamics (pt. 1), (Wiley: New York) 1968, Chapter 3.
12. W. H. Rohsenow and H. Y. Choi, Heat, Mass, and Momentum Transfer (Prentice Hall: New York), 1961, Chapter 3.
13. H. Lamb, Hydrodynamics (Dover: New York) 1945, Section 274.
14. S. H. Davis, *J. Fluid Mech.* **98**, 225-242 (1980).
15. M. Gunji, T. B. Jones, and M. Washizu, *Proc. IEJ-ESA Joint Symposium on Electrostatics*, Kyoto, Japan, 78-87 (2000).
16. J. R. Melcher and M. Hurwitz, *J. Spacecr. Rockets* **4**, 864-881 (1967).
17. S. Schiaffino and A. A. Sonin, *J. Fluid Mech.* **343**, 95-110 (1997).
18. M. Vallet, M. Vallade, and B. Berge, *Eur. Phys. J. B* **11**, 583-591 (1999).
19. L. D. Landau and E. M. Lifshitz, Electrodynamics of Continuous Media, (trans. by J. B. Sykes and J. S. Bell), (Pergamon: Oxford) 1960, p. 64-69.
20. C. E. Rosenkilde, *Proc. Royal Soc.* (London) **A312**, 473 (1969)
21. H. H. Woodson and J. R. Melcher, Electromechanical Dynamics (pt. 2), (Wiley: New York) 1968, Chapter 8.

APPENDIX – ELECTRICAL SURFACE TRACTION

The starting point for the theory of liquid DEP is the Kelvin-Helmholtz formulation for the volume force density [19].

$$\vec{f}^{\,e} = \rho_f \vec{E} - \tfrac{1}{2} E^2 \nabla \varepsilon + \nabla\left(\tfrac{1}{2} E^2 \rho \frac{\partial \varepsilon}{\partial \rho}\right) \qquad \text{(A1)}$$

where ρ_f is volume charge density. The associated Maxwell stress tensor is

$$T^e_{mn} = \varepsilon E_m E_n - \tfrac{1}{2}\delta_{mn} E_k E_k \left[\varepsilon - \rho\left(\partial\varepsilon/\partial\rho\right)\right] \qquad \text{(A2)}$$

The term involving $\partial\varepsilon/\partial\rho$ represents electrostriction, and, in the case of common liquids, which are virtually incompressible under normal conditions, its influence on hydrostatics may be ignored [20]. We further assume no free charge is present: $\rho_f = 0$. Then, if the

liquid is homogeneous, this formulation places the DEP force at interfaces and a modified Bernoulli equation may be used.

$$\left[p + \rho g z\right] - \frac{1}{2} E^2 \quad \varepsilon = 0 \qquad \text{(A3)}$$

Here, p is hydrostatic pressure and z is vertical elevation. Within the liquid, the term $p + \rho g z$ is constant, but at interfaces, the apparent DEP surface force can support hydrostatic pressure discontinuities, including capillarity and electrical force contributions. For the water finger depicted in Fig. 1, the electric field at the surface is essentially tangential. Letting this field quantity be E_t, the pressure difference is:

$$p_{\text{liquid}} - p_{\text{air}} = \gamma\left(1/R\right) + T^e \qquad \text{(A4)}$$

where

$$T^e \equiv T^e_{zz}\Big|_{\text{liquid}} - T^e_{zz}\Big|_{\text{air}} = -\frac{1}{2}\left(\varepsilon - \varepsilon_o\right) E_t^2 \qquad \text{(A5)}$$

is the electric surface traction as defined by Woodson and Melcher [21].